OCT Image Analysis of Internal Changes in Leaves due to Ozone Stresses

Hayate Goto[1][a], Nofel Lagrosas[2][b] and Tatsuo Shiina[1][c]

1Chiba University, Yayoi-cho, Inage-ku, Chiba-shi, Chiba, Japan
2School of Engineering, Kyushu University, 744 Motooka, Nishi-ku, Fukuoka, Japan

Keywords: OCT, Indicator Plant, Environmental Assessment, Ozone, GLCM.

Abstract: Changes in environmental conditions can be evaluated by detecting the conditions in indicator plants. Indicator plants are sensitive to specific environmental stresses. This research focused on white clover as an indicator plant for ozone. To analyze the effects of weaker stresses, compact OCT (Optical coherence tomography) for plants was developed, which allows for non-invasive and non-contact cross-sectional imaging of white clover (*Trifolium repens*) leaves exposed to ozone gas. OCT image changes on each level of ozone damage were evaluated using parameters such as the OCT signal level of the leaf palisade layer, the thickness of the leaf palisade layer, and texture analysis using GLCM (Gray-Level Co-occurrence Matrix). Measurements of leaves grown in our laboratory showed increased palisade tissue signal, thicker palisade tissue, a smaller distribution of palisade layer thickness, increased OCT image contrast, and decreased OCT image homogeneity.

1 INTRODUCTION

In Japan, due to the pollution problems caused by high economic growth around the 1950s, it became clear that plants were affected by air pollution (Takeshi, 2020). Using plants to help evaluate the atmospheric environment is attracting attention. Indicator plants are sensitive to specific environmental stresses which can provide vital information on the local environmental conditions. For example, white clover is an indicator plant for ozone, and white spots of visible damage occur near the leaf's main veins when exposed to high concentrations of ozone gas. Ozone concentrations can be high in urban areas due to the influence of traffic. There are significant differences in ozone concentrations between rural and urban areas.

The white clover in the field is greatly affected by ozone, and it is possible to quickly estimate the environment by observing its leaves. Indicator plants are generally evaluated by visual inspection, satellite observation, and spectroscopic observation. Spectroscopic observations can observe a decrease in the chlorophyll of the plants. However, this phenomenon is caused by dryness, insect damage, and nutritional deficiencies, and it is challenging to elucidate the cause of the change in the experimental results(Takeshi, 2020).

Optical coherence tomography (OCT) can detect morphological and intracellular tomographic images using near-infrared light (Huang et al., 1991). The internal change in plants is related to specific environmental stresses or diseases. Additionally, since OCT is an in-situ and non-invasive technique, it can be used to observe indicator plants in long-term changes over time (Wijesinghe et al., 2017; Lee et al., 2019). Recent studies showed that OCT is used in ophthalmology (Drexler et al., 2001; Wojtkowski et al., 2005; Chopra, 2022), dentistry (Sinescu et al., 2008; Colston et al., 1998), and dermatology (Liu et al., 2020; Gambichler et al., 2005). OCT is also used for observation of seed germination process (De Silva et al., 2021; Saleah et al., 2022) and diagnosis of vegetables and fruits (Zhou et al., 2022; Saleah et al., 2022; Gocławski et al., 2017). Compared to technologies that visualize internal structures, such as

a [ID] https://orcid.org/0000-0001-5387-9109
b [ID] https://orcid.org/0000-0002-8672-4717
c [ID] https://orcid.org/0000-0001-9292-4523

65

MRI and X-rays, OCT is high resolution, and capable of non-invasive quantitative analysis. Since the developed OCT is compact to bring outside, plant internal structures can be measured at growing area. Environmental conditions can assess to measuring the indicator plant in the growth area.

Ozone is purposely absorbed by the plant through its stomata which destroys the palisade tissue near the adaxial epidermis. In our previous study, white clover was exposed to high concentrations of ozone gas, and it was confirmed that the OCT signal decreased measured above the palisade tissue (Goto et al., 2023). To evaluate the internal changes caused by ozone, this research extracted features from the OCT images of white clover leaves.

This study aimed to explore OCT signal processing and image analysis methods for classifying the level of environmental damage to white clover leaves using machine learning. Since the effect of ozone gas is likely to appear in the thickness and OCT image texture of the palisade tissue, we performed thickness evaluation by layer detection using peak detection and OCT image texture analysis and developed the optimum feature extraction for OCT signal analysis.

2 METHOD

2.1 Developed Plant OCT System

The developed plant time domain (TD)-OCT system is based on a Michelson interferometer (Fig.1). The light irradiated from the super luminescent diode (SLD (ANRITSU, AS3E113HJ10M)) light source is split into a reference optical path and a sample optical path by a fiber coupler. The light returning from the sample optical path has different optical path lengths due to the light backscattered by different layers within the sample leaf. The reference optical path length changes at a constant speed, performing the rotation mechanism (Fig.2). The light path in the reference optical path (red arrow) is shown in Figure 2. The light comes from the light upper position, returns to the same position, and goes back to the fiber coupler. To rotate the mirror on the stage, the reference optical path length is changed. Since low-coherence light is used, the intensity of the interference light can be observed only when the optical path lengths match within the coherence length. Since the reference optical path length changes linearly with time, linear analysis can be conducted directly (Shiina et al., 2003; Saeki et al., 2021).
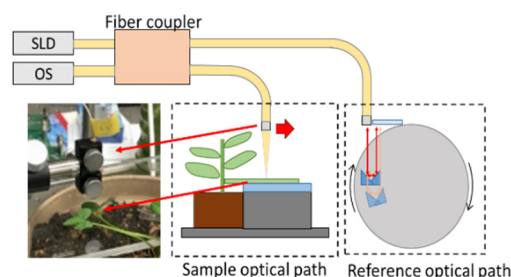

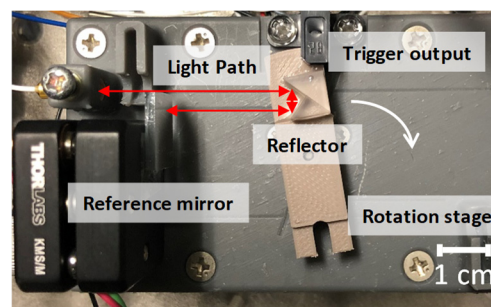Figure 1: The configuration of the plant OCT system.

Figure 2: Reference optical path system.

Table 1: Specification of OCT system.

Parameters	Values
Center wavelength	1310 nm
FWHM	53 nm
SLD output	15μW
Axial resolution	14.2 μm
Lateral resolution	10 μm
A-scan rate	25 Hz
OCT size	198×168×98 mm
Probe size	φ6 mm×9 mm

Table 1 shows the characteristics of the developed OCT (Goto et al., 2023). The central wavelength is 1310 nm, which has low absorption by chlorophyll and the local minimum value of the absorption by water. The axial resolution is 14.2 μm related to SLD coherent length. At 1310 nm, the resolution is lower than that of light wavelength around 800 nm, which is commonly used in medical OCT, but the measuring depth is more extended because it is less affected by scattering and absorption. The signal acquisition rate is 25 Hz, and 16 accumulated signals were averaged to collect one A-line data which reduces noise. The probe moves every 10 μm to produce an image from 400 signals. The size of OCT is small enough to be carried outside and measured in the field.

2.2 Exposure to Ozone Gas

White clover was grown in an incubator at 20°C with an ozone generator (KENWOOD, CAX-DM01) at a concentration of 0.17-0.21 ppm. The red and blue light of the cold cathode lamp that is easy to absorb by plant's leaves is irradiated for 15 hours a day inside the incubator. Measurements were done before placing plants in the incubator and after placing plants in the incubator every 3, 6, 10, and 14 days. The plants were measured in growing conditions to analyze effects within the same leaf.

2.3 Parameter Extraction

To confirm the influence of ozone, multiple analysis parameters were utilized by measuring the intensity of the OCT signal, the thickness of the palisade structure using peak detection, and texture analysis using the Gray-Level Co-occurrence Matrix (GLCM) within the palisade structure.

2.3.1 The Intensity of Palisade Tissue

To obtain the OCT interference intensity of the palisade tissue, the acquired data was processed by background subtraction, focal length correction, and distance squared correction. To make one A-line, 400 A-lines were aligned and averaged. The averaged A-line was performed by using normalization with the maximum value, and logarithmic transformation. Figure 3 shows the OCT signal change in the A-line before and after 10 days of exposure to ozone gas. The x-axis is the depth of the sample leaves, and the y-axis is the logarithmic intensity of the OCT signal. The green line in Fig.3 is before exposure to ozone, the yellow line is after ten days of exposure to ozone. This graph shows smooth lines because averaging to evaluate the change in a whole image of a leaf itself. The first minimum value after the maximum position (red dots points in Fig. 3) was defined as the intensity of the middle position of the palisade layer.

2.3.2 Thickness Calculations

Figure 4 shows the flowchart of the thickness calculation program. This program selects the positions of the first and second peaks. Since the first peak is the surface layer, and the second peak is the palisade and spongy layer boundary, the difference between these peaks is considered as the palisade layer thickness.

Peak detection was performed using Matlab's PeakFinder command (Fig.5). The x-axis shows the depth information of the leaf, and the y-axis shows
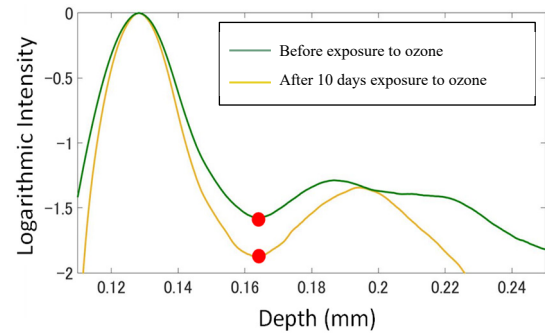

Figure 3: The signal comparison in the palisade layer before and after exposed to ozone gas.
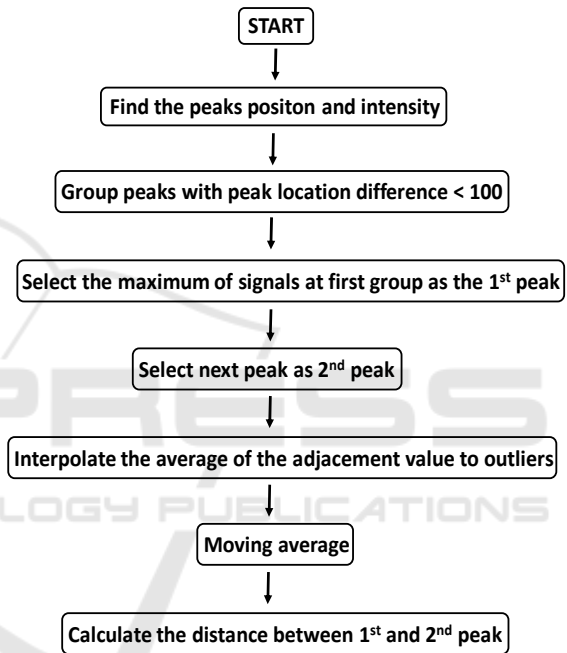

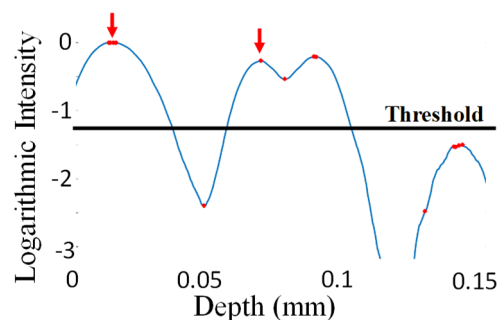Figure 4: Flowchart of thickness calculations.

Figure 5: Peak detection of A-line.

the logarithmic intensity of the OCT signal. At this time, a threshold value was used to prevent peaks below a particular value. After that, all of the A-line peaks in the OCT images were detected. The outliers
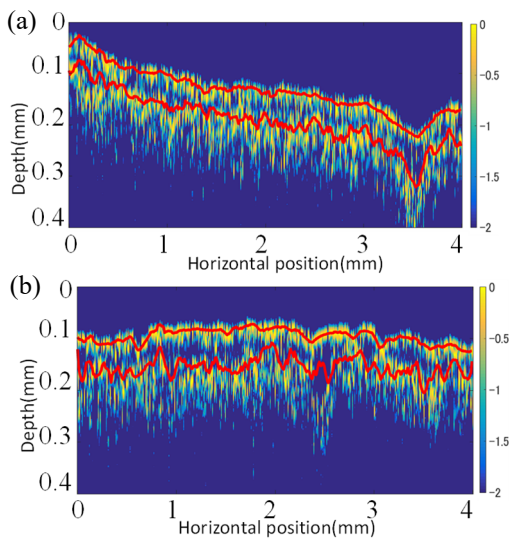
Figure 6: Peak detection of B-scan image (a) Before exposure to ozone gas and (b) After 10 days exposure to ozone gas.

of peak positions in the images were removed and interpolated. The moving average was taken so the peak detection results fit smoothly with the OCTimage. Finally, we obtained the distance between the two peaks and made a histogram. The red arrow indicates the peak point that is defined by this method.

Figure 6(a) and 6(b) show the results of peak detection before and after exposure to ozone gas, respectively. The image's upper part is the leaf's adaxial surface, and measurements are taken with light incident from this direction. The x-axis is the scanning direction, and the y-axis is the depth direction of the white clover leaf. The image's aspect ratio has been changed to make it easier to see peak detection results. The red line in the image is the result of peak detection, and it can be confirmed that the two layers can be detected correctly. Since the ozone gas destroys the palisade tissue, the two peaks in Figure 6(b) have a larger distance than the two peaks in Figure 6(a).

From each histogram, the kurtosis, which indicates the degree of concentration of the distribution, and the average value were obtained and compared with the measurement results of white clover leaves grown under each condition.

Figure 7 is an example of the histogram. The blue bar graph is the result before exposure to ozone gas, and the red bar graph is the result after 10 days of exposure to ozone gas. A detailed discussion of Figure 7 is shown in subsection 3.2 Thickness calculation.

2.3.3 GLCM (Gray-Level Co-Occurrence Matrix)

GLCM is a method that creates a matrix from the frequency of appearance of specific pixel value pairs and evaluates the image texture of an object. In the previous OCT research, OCT images could evaluate the moisture change because of the storage using contrast, correlation, energy, and homogeneity from the GLCM matrix and classify them using machine learning of support vector machine (SVM) (Srivastava et al., 2018).

Figure 8 shows the method for making GLCM. One pixel intensity compares with the intensities of adjacent pixels. GLCM creates a matrix that counts the number of identical intensity pairs. Contrast and homogeneity were calculated using the following equations (1) and (2) using the created matrix.

$$\text{Contrast} = \sum_{i,j} |i-j|^2 \, p(i,j) \tag{1}$$

$$\text{Homogeneity} = \frac{p(i,j)}{1+|i-j|} \tag{2}$$

The i,j indicates the positions within the GLCM matrix, and p(i,j) indicates the frequency of appearance of specific pixel value pairs. μ and σ are each row and column's average and standard deviation, respectively.
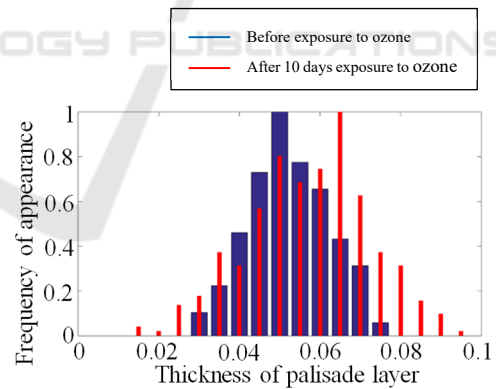

Figure 7: Histgram of the thickness.

3 RESULTS AND DISCUSSION

3.1 Intensity of Palisade Layer

Figure 9 shows the result of the intensity change inside the palisade tissues. The vertical axis indicates the differences between the epidermis surface and the middle position of palisade tissue intensity, and the horizontal axis is the day of growing in the incubator.
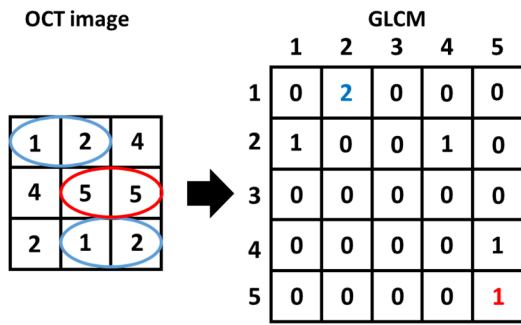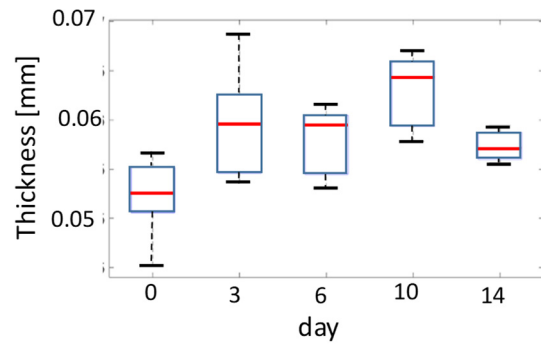
Figure 8: GLCM.

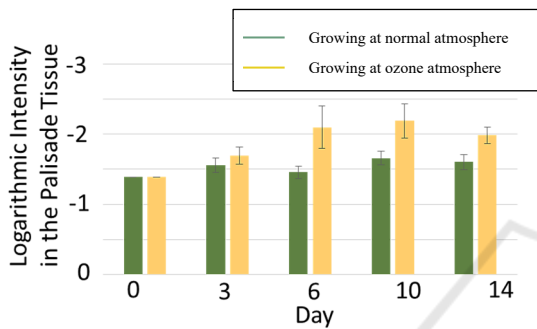Figure 10: Average thickness.

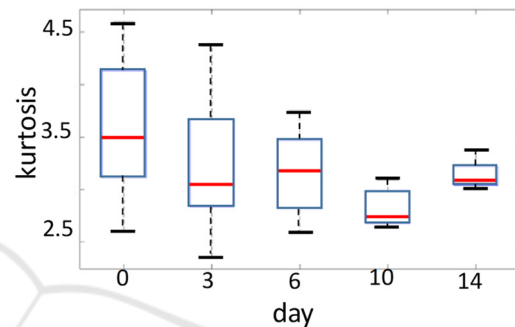
Figure 9: Average of thickness.

Figure 11: Kurtosis of thickness distribution.

The yellow bar indicates the result of growth in the high concentration of ozone gas, and the green bar indicates the result of growth in the normal air condition. Higher intensities are observed in the palisade tissues under high ozone concentration as compared to tissues under normal air conditions.

In the case of normal conditions, the intensity of palisade tissue did not have significant changes. However, in the case of a high ozone concentration, the palisade tissue intensity became higher from Day 0 to Day 10. Ozone gas enters the inside of leaves from the stoma and generates the reactive oxygen species (Takeshi, 2020). Since the oxidation stress occurs due to the reactive oxygen species, the palisade tissue is highly affected by ozone as compared to spongy tissue. The less scattering effect observed inside the destroyed leaf palisade tissue leads to a lower signal.

Comparing the ozone exposure result of Day 0 with other days except for Day 10 in Figure 9 using a t-test, a significant change didn't appear in the normal air conditions (Day 3 : p = 0.140, Day 6 : p = 0.460, Day 10 : p = 0.021, Day 14 : p = 0.059). Day 10 result shows a significant change compared to Day 0 because of the growth or senescence. On the other hand, a significant change was observed from Day 0 to later days (Day 3: p = 0.037, Day 6 : p = 0.047, Day 10 : p = 0.012, Day 14 : p = 0.000064) after exposure

to ozone gas. In this research, visible inspection where white spots appear near the leaf's main vein can be observed after 10 days of exposure to ozone gas. Thus, the indicator plants measurement using OCT can detect the leaf change after 3 days of exposure to ozone gas, and it is earlier than visible inspection. OCT can detect the early stage of the inspection and small inspection due to environmental stresses or diseases.

3.2 Thickness Calculations

Figure 7 shows the histogram of leaf thickness after 0 and 10 days of exposure to ozone gas. This thickness value was calculated as described in subsection '2.3.2 Thickness calculations' in the section '2 METHOD'. The median value of the thickness in 10 days became thicker than the median value in 0 days. The 10-day histogram has a wider distribution than the 0-day histogram due to the ozone gas effect.

Figures 10 and 11 show the average and kurtosis of the thickness measured from the OCT image, respectively. The horizontal axis is the day of growing in the incubator, and the vertical axis is the average and kurtosis of the thickness. As observed, the average thickness increases, and the kurtosis decreases during the sampling period. Since the part of destroyed tissue by ozone was filled with water, the
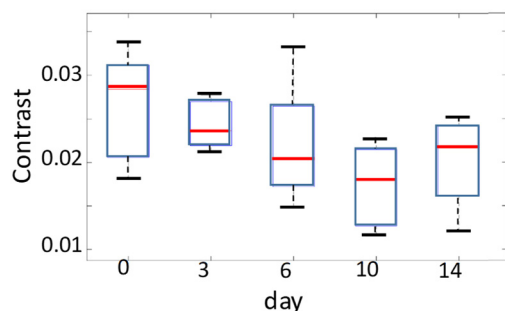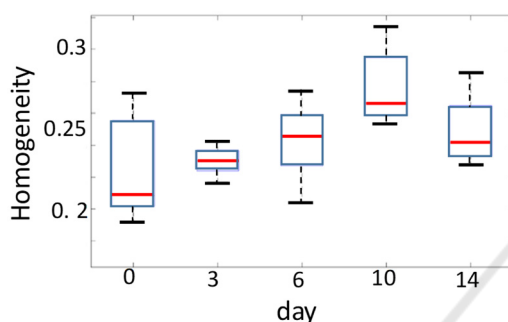
Figure 12: Contrast of palisade layer.

Figure 13: Homogeneity of palisade layer.

intercellular space expanded, and the thickness of palisade tissue increased as shown in Figure 10. The decrease of kurtosis is due to the morphological changes in the leaf. As the influence of the ozone effect increased, the damaged region in the leaf expanded and made a uniform condition. This caused a decrease in the distribution of thickness, and the kurtosis was decreased. The leaf at the initial state has a large variation of the kurtosis. The initial state of cells that are not damaged and have several conditions due to senescence. Additionally, the 14th-day result of an average thickness is increased, and the kurtosis of thickness distribution is decreased. It did not fit the same trend in earlier days.

3.3 GLCM

Figures 12 and 13 show the GLCM results of contrast and homogeneity, respectively. The horizontal axis is the day of growing in the incubator, and the vertical axis is the contrast and homogeneity. The contrast value is decreased and the homogeneity value is increased with the day except for 14 days result. These results showed a similar trend to the thickness results (Fig. 10 and 11). This confirms that the palisade tissues were destroyed and filled with water upon exposure to ozone gas. As observed in the OCT images, the water part showed less contrast and high homogeneity compared with the cell part.

Day 14 has the other trend same as Figures 10 and 11 such as high contrast and less homogeneity. The plants may become partially senescence by the ozone effect. Since this causes the dryness inside the leaf and the high scattering of the light, the thickness became thicker (Fig.10), bigger kurtosis of thickness (Fig.11), high contrast (Fig.12), and low homogeneity (Fig.13).

4 CONCLUSIONS

In this study, we examined the possibility of the white clover leaves as an indicator plant for ozone gas using TD-OCT. This study shows the use of OCT as an early detection device for ozone gas. If the plant leaves are exposed to ozone gas, ozone gas enters inside the leaves from the stoma and destroys the palisade tissue. This phenomenon causes the OCT intensity to decrease in the palisade tissue. This study performed peak detection and texture analysis to evaluate the effects of ozone gas on white clover leaves. Additionally, the thickness of palisade tissue became thicker and has smaller distribution. The GLCM result of palisade tissue has low contrast and high homogeneity. After 14 days of exposure to ozone gas, due to necrosis, they showed other trends compared to before 14 days.

To classify the degree of damage caused by ozone gas, this research will increase the number of samples and use machine learning for classification. To distinguish the ozone effect from other stresses, the plants will be measured and evaluated under other conditions such as dryness, lack of nutrients, lack of light, and varying temperatures. The parameters such as interfered intensity of palisade tissue, thickness distribution of the palisade tissue, and image texture that only appeared in the ozone effect will be selected for evaluation of the condition of the plant growing area.

Using OCT in the field, the relationship between the field conditions and indicator plant parameters can be properly assessed. This method can be helpful in the field of agriculture research because the selection of crops to be planted, and proper application of pesticides and other growth parameters can be studied.

REFERENCES

Takeshi, I. (2020). Atmospheric environment and Plant (Taiki kankyo to syokubutu. Asakura Shoten, ISBN 987-4-254-42045-6 C 3061 ,Japan.

Huang, D., Swanson, E. A., Lin, C. P., Schuman, J. S., Stinson, W. G., Chang, W., Hee, M. R., Flotte, T., Gregory, K., & Puliafito, C. A. (1991). Optical coherence tomography. *Science (New York, N.Y.)*, *254*(5035), 1178–1181.

Drexler, W., Morgner, U., Ghanta, R. K., Kärtner, F. X., Schuman, J. S., & Fujimoto, J. G. (2001). Ultrahigh-resolution ophthalmic optical coherence tomography. *Nature medicine*, *7*(4), 502–507.

Wojtkowski, M., Srinivasan, V., Fujimoto, J. G., Ko, T., Schuman, J. S., Kowalczyk, A., & Duker, J. S. (2005). Three-dimensional retinal imaging with high-speed ultrahigh-resolution optical coherence tomography. *Ophthalmology*, *112*(10), 1734–1746.

Chopra V. (2022). Association of Rates of Optical Coherence Tomography Angiography Vessel Density Loss on Initial Visits With Future Visual Field Progression. *JAMA ophthalmology*, *140*(4), 326–327.

Sinescu, C., Negrutiu, M. L., Todea, C., Balabuc, C., Filip, L., Rominu, R., Bradu, A., Hughes, M., & Podoleanu, A. G. (2008). Quality assessment of dental treatments using en-face optical coherence tomography. *Journal of biomedical optics*, *13*(5), 054065.

Colston, B., Sathyam, U., Dasilva, L., Everett, M., Stroeve, P., & Otis, L. (1998). Dental OCT. *Optics express*, *3*(6), 230–238.

Liu, Y., Zhu, D., Xu, J., Wang, Y., Feng, W., Chen, D., Li, Y., Liu, H., Guo, X., Qiu, H., & Gu, Y. (2020). Penetration-enhanced optical coherence tomography angiography with optical clearing agent for clinical evaluation of human skin. *Photodiagnosis and photodynamic therapy*, *30*, 101734.

Gambichler, T., Moussa, G., Sand, M., Sand, D., Altmeyer, P., & Hoffmann, K. (2005). Applications of optical coherence tomography in dermatology. *Journal of dermatological science*, *40*(2), 85–94.

De Silva, Y. S. K., Rajagopalan, U. M., Kadono, H., & Li, D. (2021). Positive and negative phenotyping of increasing Zn concentrations by Biospeckle Optical Coherence Tomography in speedy monitoring on lentil (Lens culinaris) seed germination and seedling growth. *Plant Stress*, 2, 100041.

Saleah, S. A., Lee, S. Y., Wijesinghe, R. E., Lee, J., Seong, D., Ravichandran, N. K., Jung, H. Y., Jeon, M., & Kim, J. (2022). Optical signal intensity incorporated rice seed cultivar classification using optical coherence tomography. *Computers and Electronics in Agriculture*, 198, 107014.

Zhou, Y., Wu, Y., & Chen, Z. (2022). Detection of Mold-Contaminated Maize Kernels Based on Optical Coherence Tomography. *Food Anal. Methods*, 15, 1619-1625.

Saleah, S. A., Wijesinghe, R. E., Lee, S. Y., Ravichandran, N. K., Seong, D., Jung, H. Y., Jeon, M., & Kim, J. (2022). On-field optical imaging data for the pre-identification and estimation of leaf deformities. *Scientific data*, *9*(1), 698.

Gocławski, J., Nalewajko, J. S., Korzeniewsk, E.,& Piekarsk, A. (2017). The use of optical coherence tomography for the evaluation of textural changes of grapes exposed to pulsed electric field. *Computers and Electronics in Agriculture*, 142, 29-40.

Wijesinghe, R. E., Lee, S. Y., Ravichandran, N. K., Han, S., Jeong, H., Han, Y., Jung, H. Y., Kim, P., Jeon, M., & Kim, J. (2017). Optical coherence tomography-integrated, wearable (backpack-type), compact diagnostic imaging modality for in situ leaf quality assessment. *Applied optics*, *56*(9), D108–D114.

Lee, J., Lee, S. Y., Wijesinghe, R. E., Ravichandran, N. K., Han, S., Kim, P., Jeon, M., Jung, H. Y., & Kim, J. (2019). On-Field In situ Inspection for Marssonina Coronaria Infected Apple Blotch Based on Non-Invasive Bio-Photonic Imaging Module. *IEEE Access*, 7, 148684-148691.

Goto, H., & Shiina, T. (2023). Environmental Pollution Assessment with Indicator Plant Under Ozone Gas Atmosphere by Using OCT. *Proceedings of the 11th International Conference on Photonics, Optics and Laser Technology*, 1, PHOTOPTICS, 34-39.

Shiina, T., Moritani, Y., Ito, M., & Okamura, Y. (2003). Long-optical-path scanning mechanism for optical coherence tomography. *Applied optics*, *42*(19), 3795–3799.

Saeki, K., Huyan, D., Sawada, M., Nakamura, A., Kubota, S., Uno, K., Ohnuma, K., & Shiina, T. (2021). Three-dimensional measurement for spherical and nonspherical shapes of contact lenses. *Applied optics*, *60*(13), 3689–3698.

Srivastava, V., Dalal, D., Kumar, A., Prakash, S., & Dalal, K. (2018). In vivo automated quantification of quality of apples during storage using optical coherence tomography images. *Laser Physics*, 28, 066207